

Fast Directional Computation for the High Frequency Helmholtz Kernel in Two Dimensions

Björn Engquist and Lexing Ying
Department of Mathematics, University of Texas, Austin, TX 78712

February 2008

Abstract

This paper introduces a directional multiscale algorithm for the two dimensional N -body problem of the Helmholtz kernel with applications to high frequency scattering. The algorithm follows the approach in [Engquist and Ying, SIAM Journal on Scientific Computing, 29 (4), 2007] where the three dimensional case was studied. The main observation is that, for two regions that follow a directional parabolic geometric configuration, the interaction between the points in these two regions through the Helmholtz kernel is approximately low rank. We propose an improved randomized procedure for generating the low rank representations. Based on these representations, we organize the computation of the far field interaction in a multidirectional and multiscale way to achieve maximum efficiency. The proposed algorithm is accurate and has the optimal $O(N \log N)$ complexity for problems from two dimensional scattering applications. We present numerical results for several test examples to illustrate the algorithm and its application to two dimensional high frequency scattering problems.

Keywords. N -body problems; Helmholtz equation; Oscillatory kernels; Fast multipole methods; Multidirectional computation; Multiscale methods.

AMS subject classifications. 65N38; 65R20.

1 Introduction

1.1 Problem statement

In this paper, we consider the two dimensional N -body problem for the high frequency Helmholtz kernel. Let $\{f_i, 1 \leq i \leq N\}$ be a set of charges located at points $\{p_i, 1 \leq i \leq N\}$ in \mathbb{R}^2 . We assume that the points $\{p_i\}$ belong to a square centered at the origin with size K . The problem is to evaluate the potentials $\{u_i, 1 \leq i \leq N\}$ defined by

$$u_i = \sum_{j=1}^N G(p_i, p_j) \cdot f_j \quad (1)$$

where $G(x, y) = \frac{\iota}{4} H_0^{(1)}(2\pi|x-y|)$ is the fundamental solution of the 2D Helmholtz equation. In this paper, we use ι to denote $\sqrt{-1}$.

This computational problem mostly arises from the numerical solution of 2D time harmonic scattering problems [9]. For example, suppose that $D \subset \mathbb{R}^2$ is a compact object with a smooth boundary and u^{inc} is the incoming field. If D represents a sound soft scatterer,

the scattering field u satisfies the following Helmholtz equation with the Dirichlet boundary condition:

$$\begin{aligned} -\Delta u - (2\pi)^2 u &= 0 \quad \text{in } \mathbb{R}^d \setminus \bar{D} \\ u(x) &= -u^{inc}(x) \quad \text{for } x \in \partial D \\ \lim_{r \rightarrow \infty} r \left(\frac{\partial u}{\partial r} - 2\pi i u \right) &= 0 \end{aligned}$$

where the wave number is set to be 2π . The last condition is the Sommerfeld radiation condition and guarantees that the scattering field u propagates to infinity. One highly efficient way to solve this problem is to reformulate it into an equivalent boundary integral equation (BIE)

$$\frac{1}{2}\phi(x) + \int_{\partial D} \left(\frac{\partial G(x, y)}{\partial n(y)} - \eta G(x, y) \right) \phi(y) dy = -u^{inc}(x) \quad (2)$$

where $n(y)$ is the exterior normal of ∂D at y , η is some fixed constant, and $\phi(x)$ for $x \in \partial D$ is the unknown charge distribution on the boundary ∂D . Once ϕ is solved from (2), the scattering field u can be simply computed with an integral formula [9]. The BIE approach has the advantage of reducing the number of unknowns. The discrete version of (2), however, is a dense linear system which usually requires an iterative algorithm like GMRES [28] for its solution. At each step of the iterative solver, we then need to evaluate the computational problem in (1), with $\{p_i\}$ being the appropriate quadrature points.

It is well known that the complexity of a scattering problem often scales with the size of scatterer in terms of the wavelength. Since the wavelength is taken to be 1 in our setup, the complexity of (1) depends on the number K , which can be of order 10^4 for a typical large scale scattering problem. Since one often uses a constant number of points per wavelength when discretizing (2), the number of points N is proportional to K .

1.2 Previous work

Direct computation of (1) takes $O(N^2)$ operations. This can be quite time consuming when N is large. Various fast algorithms have been proposed to reduce this complexity in the past two decades. Among them, the most popular approach is the high frequency fast multipole method (HF-FMM) developed by Rokhlin et al. [7, 27]. In the HF-FMM, the whole computational domain is partitioned into a quadtree and one associates with each square of the quadtree two expansions: the far field expansion and the local field expansion [7]. These expansions allow one to accelerate the computation in the low frequency region. In the high frequency region, the Fourier transforms of these expansions are used instead to achieve optimal efficiency since the translations between them become diagonal operators under the Fourier basis. The HF-FMM has an optimal $O(N \log N)$ complexity and has been widely used.

A different approach is to discretize the integral equation (2) under the Galerkin framework using local Fourier bases or wavelet packets. The stiffness matrix becomes approximately sparse under these bases since most of the entries are close to zero and can be safely discarded. Early algorithms [2, 4, 6, 11, 12, 16] of this approach focus on finding the correct one dimensional basis, while a recent development [20] considers the use of two dimensional wave packets which can offer more flexibility and better compression rate.

Another early development is the multilevel matrix decomposition by Michielssen and Boag [25]. The three stage multiplication algorithm, which is later named the butterfly

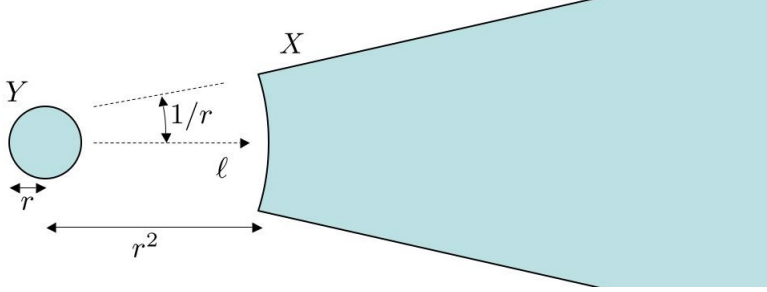


Figure 1: Two sets Y and X that satisfy the directional parabolic separation condition.

algorithm by [26], is quite similar to the FFT and brings the overall complexity down to $O(N \log^2 N)$.

In [15], we proposed an algorithm for the three dimensional N -body problem of the high frequency Helmholtz kernel. It relies on a low rank property of the 3D Helmholtz kernel for certain geometric configurations. The algorithm organizes the computation in a multidirectional and multilevel fashion and has an optimal $O(N \log N)$ complexity.

1.3 A multidirectional approach

In this paper, we adapt the approach in [15] to the two dimensional N -body problem of the Helmholtz kernel. The main idea is a similar low rank property of the 2D Helmholtz kernel. We say that two sets Y and X satisfy the *directional parabolic separation condition* if Y is a disk of radius r and X is the set of points that belong to a cone with spanning angle $1/r$ and are at least r^2 away from Y (see Figure 1).

Once Y and X satisfy the directional parabolic separation condition, one can show that for any fixed accuracy the interaction between X and Y via the Helmholtz kernel $G(x, y)$ is approximately of low rank and the rank is independent of r . More precisely, for any accuracy ε , there exist a constant $T(\varepsilon)$ and two sets of functions $\{\alpha_i(x), 1 \leq i \leq T(\varepsilon)\}$ and $\{\beta_i(y), 1 \leq i \leq T(\varepsilon)\}$ such that for any $x \in X$ and $y \in Y$

$$\left| G(x, y) - \sum_{i=1}^{T(\varepsilon)} \alpha_i(x) \beta_i(y) \right| \leq \varepsilon$$

(see Theorem 2.2). Notice that $\{\alpha_i(x)\}$ and $\{\beta_i(y)\}$ are only functions of x and y respectively. We call such an approximation a *directional separated representation*. One major component of our approach is to use these representations to build equivalent charges for well-separated interaction.

Similar to the 3D algorithm in [15], our 2D algorithm starts by generating a quadtree for the whole computational domain. In the low frequency region where the squares are of size less than 1, the interactions are accelerated using the kernel independent FMM algorithm in [30]. In the high frequency region where the squares are of size greater than or equal to 1, the far field of each square is partitioned into wedges which follow the directional parabolic separation condition (see Figure 2). Between the square and each of its wedges, the computation is accelerated via the directional separated representation associated with the wedge.

Apart from extending the multidirectional algorithm of [15] to the 2D Helmholtz kernel, this paper also contains two new contributions:

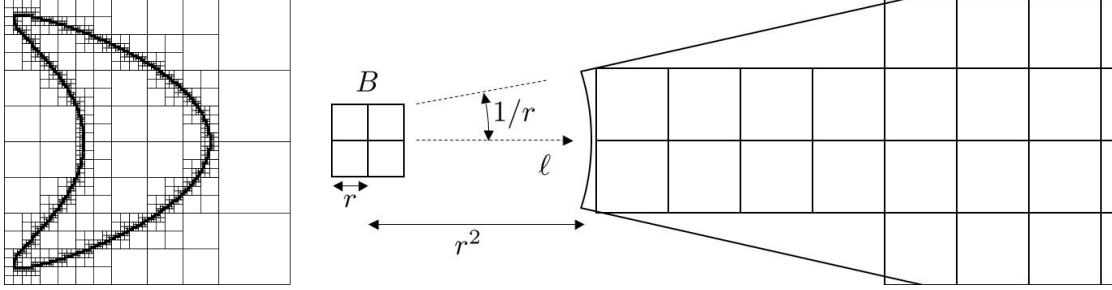


Figure 2: Left: the quadtree constructed for a point distribution supported on a curve. Right: for each square B in the high frequency region, its far field is partitioned into multiple wedges. We construct a low rank representation of the interaction between B and each of its wedges. This representation is further used to accelerate the computation between B and all the squares in the wedge.

- We provide an improved randomized procedure for the construction of the directional separated representations. The new procedure is more efficient and generates representations with smaller ranks.
- Our algorithm has been applied to the solution of (2). This allows us to study large scatterers that are thousands of wavelengths wide.

The rest of this paper is organized as follows. In Section 2, we briefly summarize the theoretical result on which our approach is based and describe the new improved procedure for constructing the separated representations. After describing our algorithm for (1) in detail in Section 3, we present in Section 4 the numerical results for several test examples. Finally, Section 5 provides some comments on future research directions. Though this paper focuses on the two dimensional Helmholtz kernel, we would like to point out that our algorithm is also applicable to other 2D oscillatory kernels such as $e^{2\pi i|x-y|}$.

2 Directional Separated Representations

Definition 2.1. Let $f(x, y)$ be a function for $x \in X$ and $y \in Y$. We say $f(x, y)$ has a T -term ε -expansion for X and Y if there exist functions $\{\alpha_i(x), 1 \leq i \leq T\}$ and $\{\beta_i(y), 1 \leq i \leq T\}$ such that

$$\left| f(x, y) - \sum_{i=1}^T \alpha_i(x) \beta_i(y) \right| \leq \varepsilon$$

for all $x \in X$ and $y \in Y$.

Since the two sets of functions $\{\alpha_i(x)\}$ and $\{\beta_i(y)\}$ depend only on x and y respectively, the above expansion is called *separated*. Suppose $r \geq \sqrt{2}$. For our problem, we take

$$Y = B(0, r) \quad \text{and} \quad X = \{x : \theta(x, \ell) \leq 1/r, |x| \geq r^2\} \quad (3)$$

where ℓ is a given unit vector and $\theta(a, b)$ is the spanning angle between vectors a and b . The geometric relationship between Y and X is illustrated in Figure 1. The following theorem serves as the theoretical foundation of our approach.

Theorem 2.2. For any $\varepsilon > 0$, there exists a number $T(\varepsilon)$ which is independent of r such that

$$G(x, y) = \frac{i}{4} H_0^{(1)}(2\pi|x - y|)$$

has a $T(\varepsilon)$ -term ε -expansion for any X and Y given by (3).

The representation guaranteed by Theorem 2.2 is called a *directional separated representations* for the obvious reason. One way to prove this theorem is to use the asymptotic behavior of $H_0^{(1)}$ for large arguments [1, 5]:

$$H_0^{(1)}(r) = \sqrt{\frac{2}{\pi r}} \left(e^{i(r - \pi/4)} + O\left(\frac{1}{r}\right) \right),$$

and then follow the same path as the proof for Theorem 2.2 in [15].

2.1 Construction of directional separated representation

A procedure based on random sampling has been described in [15] for the construction of these directional separated representations. In the rest of this section, we propose an improved version which gives lower separation ranks and better accuracy based on our numerical experience. For a given pair Y and X that satisfy the directional parabolic separation condition, our new procedure takes the following steps:

1. Sample Y randomly with a set of samples $\{y_j, 1 \leq j \leq N_Y\}$. In our implementation, we use 2 to 3 points per wavelength and the number of samples N_Y grows linearly with the area of Y . Sample X similarly with a set of samples $\{x_i, 1 \leq i \leq N_X\}$. Let A be the matrix defined by

$$A_{ij} = G(x_i, y_j) = \frac{i}{4} H_0^{(1)}(2\pi|x_i - y_j|),$$

for $1 \leq i \leq N_X$ and $1 \leq j \leq N_Y$. In the language of linear algebra, Theorem 2.2 states that A can be factorized, within error $O(\varepsilon)$, into the product of two matrices, the first containing $T(\varepsilon)$ columns and the second containing $T(\varepsilon)$ rows.

2. Let A_1 be the submatrix of A containing a set of N_1 randomly selected rows. Here we set $N_1 \approx 3 \cdot T(\varepsilon)$ in practice. Our goal is to find a set of $T(\varepsilon)$ columns of A_1 that has the largest $T(\varepsilon)$ -dimensional volume. Since A_1 is only of size $O(T(\varepsilon)) \times N_Y$, one can use either the interpolative decomposition [8] or the greedy standard pivoted QR factorization to find these columns. Both algorithms have an $O(N_Y)$ complexity. Suppose the pivoted QR factorization is used. We then have the decomposition

$$A_1 P_1 = Q_1 R_1,$$

where P_1 is a permutation matrix, Q_1 is orthonormal, and R_1 is upper triangular. Now identify the diagonal elements of R_1 which are less than ε and truncate the associated columns of Q_1 and rows of R_1 . Denote the resulting matrices by $Q_{1,c}$ and $R_{1,c}$. Since A_1 itself has an $O(T(\varepsilon))$ -expansion, $Q_{1,c}$ contains only $O(T(\varepsilon))$ columns in practice. Moreover, it is clear that

$$Q_{1,c} R_{1,c} = A_{1,c},$$

where $A_{1,c}$ is the submatrix containing the columns of A_1 from which the matrix $Q_{1,c}$ is generated. We denote by A_c the submatrix of A that consists of the same columns. The $O(T(\varepsilon))$ samples of Y associated with these columns are denoted $\{b_q\}$.

3. Let A_2 be a submatrix of A containing a set of N_2 randomly selected columns. We again set $N_2 \approx 3 \cdot T(\varepsilon)$. Repeat the previous step on A_2^* . As a result, we have two matrices $Q_{2,r}$ and $R_{2,r}$. $Q_{2,r}$ is orthonormal and has $O(T(\varepsilon))$ columns again, while $R_{2,r}$ is upper triangular. They satisfy the relationship

$$R_{2,r}^* Q_{2,r}^* = A_{2,r},$$

where $A_{2,r}$ is a submatrix containing appropriate rows of A . We denote by A_r the submatrix of A that consists of the same rows and by $\{a_p\}$ the $O(T(\varepsilon))$ samples of X associated with these rows (see Figure 3).

4. We randomly pick a set S of N_S rows and a set T of N_T columns. In practice, we choose N_S and N_T to be equal to $10 \cdot T(\varepsilon)$. Set A_3 to be the minor containing the elements from rows in S and columns in T , $A_{c,S}$ to be the submatrix of A_c containing the rows in S , and $A_{r,T}$ to be the submatrix of A_r containing the columns in T . Next, we choose $D = (A_{c,S})^+ A_3 (A_{r,T})^+$, where $()^+$ stands for pseudoinverse. We claim that

$$|A - A_c D A_r| = O(\varepsilon).$$

Such an approximate factorization is often called a pseudoskeleton approximation of A in the literature (see [17, 18]). Notice that the matrix D has only $O(T(\varepsilon))$ rows and columns. Denoting the entries of D by d_{qp} , we can rewrite the previous statement in the form

$$\left| G(x_i, y_j) - \sum_{p,q} G(x_i, b_q) \cdot d_{qp} \cdot G(a_p, y_j) \right| = O(\varepsilon)$$

for all x_i and y_j .

5. Finally, since $\{x_i\}$ and $\{y_j\}$ sample the sets X and Y with a constant number of points per wavelength, it is reasonable to expect

$$\left| G(x, y) - \sum_{p,q} G(x, b_q) \cdot d_{qp} \cdot G(a_p, y) \right| = O(\varepsilon) \quad (4)$$

for any $x \in X \cap B(0, K)$ and $y \in Y$.

Since both $\{a_p\}$ and $\{b_q\}$ are of order $O(T(\varepsilon))$, it is clear that (4) is a low rank separated representation. Moreover, we only need to store $\{a_p\}$, $\{b_q\}$, and D for (4), thus reducing the storage requirement dramatically. We would like to point out that recently there has been a lot of research devoted to problems similar to (4) (see [3, 13, 14, 24] for details).

This randomized procedure performs quite well in practice as we will see from the numerical results in Section 4. Though we do not yet have a proof, the following heuristic argument provides some useful insights. In the standard pseudoskeleton approximation [17, 18], an $m \times n$ matrix A has the following approximation:

$$A \approx A_c G A_r,$$

where A_c , G , and A_r are of size $m \times k$, $k \times k$, and $k \times n$ respectively. Often A_c contains the columns of A that have the largest k -dimensional volume and, similarly, A_r contains the rows with the largest k -dimensional volume. Finding these columns and rows are quite expensive if both m and n are large. Suppose now that we can project the columns

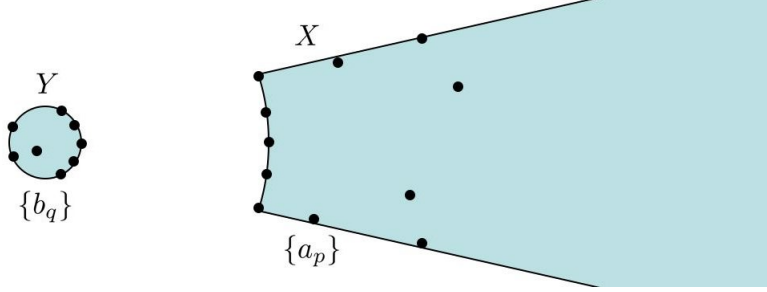


Figure 3: Constructions of the separated representation between X and Y . $\{b_q\}$ are the samples associated with the columns in A_c (Step 2). $\{a_p\}$ are the samples associated with the columns in A_r (Step 3).

(or rows) of A onto a p dimensional subspace L which is randomly selected from all p -dimensional subspaces with the uniform rotational invariant probability measure. As long as p is adequately larger than k , the volume spanned by any set of k columns (or rows) is preserved to a good accuracy [10, 23]. Therefore, one efficient method to find the columns of A with the largest volume would be to

1. project A onto a random p dimensional subspace,
2. find the columns of the projected matrix that have the largest k -dimensional volume,
3. pick the corresponding columns of A to be the answer.

The only difference between this approach and the second and third steps of our randomized procedure is that we only project to a random set of coordinates, which is much more restrictive than the uniform random projection. However, since both the columns and the rows of our matrix A is highly oscillatory and incoherent with the Dirac functions, our procedure works well in practice.

2.2 Equivalent charges

The directional separated representation (4) provides a way to represent the potential in X generated by the charges inside Y in a compact way. Suppose that X is centered around the unit direction ℓ and $\{f_i\}$ are the charges located at points $\{y_i\}$ in Y . After applying (4) to $y = y_i$ for each y_j and summing them up with weight f_i , we have

$$\left| \sum_i G(x, y_i) f_i - \sum_q G(x, b_q) \left(\sum_p d_{qp} \sum_i G(a_p, y_i) f_i \right) \right| = O(\varepsilon).$$

This states that we can place a set of charges

$$\left\{ \sum_p d_{qp} \sum_i G(a_p, y_i) f_i \right\} \tag{5}$$

at points $\{b_q\}$ in order to reproduce the potential generated by the charges $\{f_i\}$ located at points $\{y_i\}$. We call the charges in (5) the *directional outgoing equivalent charges* of Y in

direction ℓ and the points $\{b_q\}$ the *directional outgoing equivalent points* of Y in direction ℓ . In addition, we refer to the quantities

$$\left\{ \sum_i G(a_p, y_i) f_i \right\} \quad (6)$$

as the *directional outgoing check potentials* of Y in direction ℓ and the points $\{a_p\}$ as the *directional outgoing check points* of Y in direction ℓ . Given the check potentials, the equivalent charges can be computed easily by a multiplication with D .

Let us now reverse the role of X and Y . Suppose we have a set of charges $\{f_i\}$ located at points $\{x_i\}$ in X . Since $G(x, y) = G(y, x)$,

$$\left| \sum_i G(y, x_i) f_i - \sum_p G(y, a_p) \sum_q d_{qp} \sum_i G(b_q, x_i) f_i \right| = O(\varepsilon).$$

This states that we can put a set of charges

$$\left\{ \sum_q d_{qp} \sum_i G(b_q, x_i) f_i \right\} \quad (7)$$

at points $\{a_p\}$ and they reproduce the potential generated by the charges $\{f_i\}$ located at points $\{x_i\}$. Therefore, we call the charges in (7) the *directional incoming equivalent charges* of Y in direction ℓ and the locations $\{a_p\}$ the *directional incoming equivalent points* of Y in direction ℓ . In analogy to the previous terminology,

$$\left\{ \sum_i G(b_q, x_i) f_i \right\} \quad (8)$$

are called the *directional incoming check potentials* of Y in direction ℓ and the location $\{b_q\}$ are called the *directional incoming check points* of Y in direction ℓ .

3 Algorithm Description

Without loss of generality, we assume that the size of the domain $K = 2^{2L}$ for a positive integer L .

3.1 Data structure

We start by constructing a quadtree which contains the whole computational domain. We often use B to denote a square in the quadtree and w for its width. A square B is said to be in the low frequency regime if $w < 1$ and in the high frequency regime if $w \geq 1$. In the high frequency regime of the quadtree, no adaptivity is used, i.e., every non-empty square is further partitioned until the width of the square is less than 1. In the low frequency regime, a square B is partitioned as long as the number of points in B is greater than a fixed constant N_p . The value of N_p is chosen to optimize the computational complexity and, in practice, we pick $N_p = 50$.

For a square B in the low frequency regime, its data structure follows the description of the kernel independent FMM in [30]. The near field N^B is the union of the squares A that satisfies $dist(A, B) = 0$, where $dist(A, B) = \inf_{x \in A, y \in B} |x - y|$. The far field F^B is the complement of N^B . The interaction list I^B contains all the squares in $N^P \setminus N^B$ on B 's level, where P is the parent square of B .

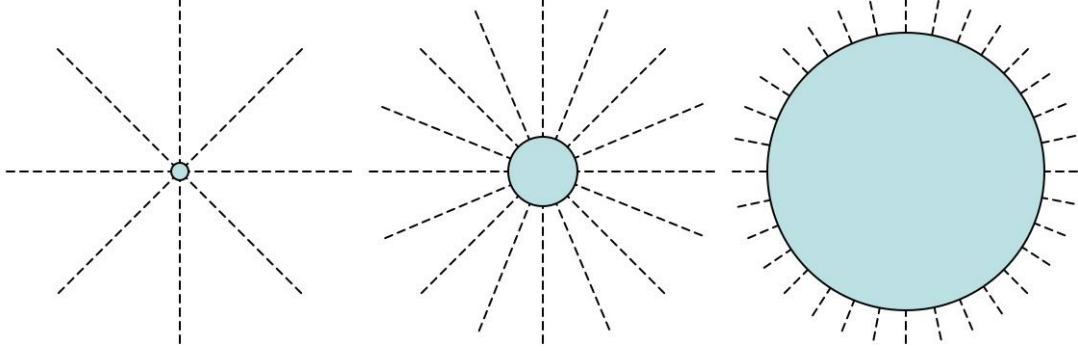


Figure 4: The far field is partitioned into wedges. From left to right, $w = 1, 2, 4$. The radii are 1, 4, and 16, respectively.

- $\{y_k^{B,o}\}$, $\{f_k^{B,o}\}$, $\{x_k^{B,o}\}$ and $\{u_k^{B,o}\}$ are, respectively, the *outgoing* equivalent points, equivalent charges, check points, and check potentials.
- $\{y_k^{B,i}\}$, $\{f_k^{B,i}\}$, $\{x_k^{B,i}\}$ and $\{u_k^{B,i}\}$ are, respectively, the *incoming* equivalent points, equivalent charges, check points, and check potentials.

For a square B in the high frequency region, the near field N^B is the union of all the squares $\{A\}$ that satisfy $dist(A, B) \leq w^2$. The far field F^B is the complement of N^B . The interaction list I^B contains all the squares in $N^P \setminus N^B$ on B 's level, where P is B 's parent square. Notice that the far field of a square B in the high frequency region is pushed away in order to be compatible with the directional parabolic separation condition. The far field F^B is further partitioned into a group of directional wedges, each belonging to a cone with spanning angle $O(1/w)$. We denote the set of all the wedges of B by $\{W^{B,\ell}\}$. In Figure 4, we illustrate the case for $w = 1, 2, 4$.

For each square B and each direction ℓ , we summarize the relevant quantities as follows:

- $\{y_k^{B,o,\ell}\}$, $\{f_k^{B,o,\ell}\}$, $\{x_k^{B,o,\ell}\}$, and $\{u_k^{B,o,\ell}\}$ are the *outgoing directional* equivalent points, equivalent charges, check points and check potentials respectively.
- $\{y_k^{B,i,\ell}\}$, $\{f_k^{B,i,\ell}\}$, $\{x_k^{B,i,\ell}\}$, and $\{u_k^{B,i,\ell}\}$ are the *incoming directional* equivalent points, equivalent charges, check points and check potentials respectively.

3.2 Translation operators

Following the convention in [19, 27], we name these operators M2M, L2L, and L2L translations, though no multipole or local expansions are involved in our algorithm. The translation operators for squares in the low frequency regime are detailed already in [30]. The operators in the high frequency regime are more complicated. The main reason is that the computations are now directional.

For a square B in the high frequency regime, the *M2M translation* constructs the outgoing directional equivalent charges of B from the outgoing equivalent charges of B 's children. There are two cases to consider. In the first case, $w = 1$. The children squares have only nondirectional equivalent charges. The M2M translation iterates over all of the directional indices $\{\ell\}$ of B , and the steps for a fixed direction ℓ are as follows:

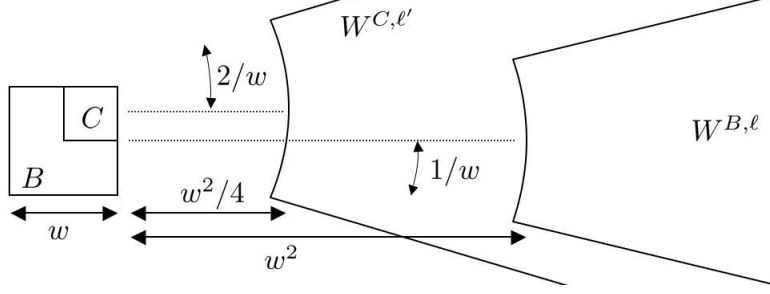


Figure 5: B is a square with width $w > 1$. For any fixed ℓ , there exists ℓ' such that $W^{B,\ell}$ is contained in $W^{C,\ell'}$ where C is any one of B 's children.

1. Use $\bigcup_C \{y_k^{C,o}\}$ as source points in B and $\bigcup_C \{f_k^{C,o}\}$ as source charges. Here the union is taken over all of the children squares of B .
2. Compute $\{u_k^{B,o,\ell}\}$ at points $\{x_k^{B,o,\ell}\}$ with kernel evaluation, and then obtain $\{f_k^{B,o,\ell}\}$ by multiplying $\{u_k^{B,o,\ell}\}$ with the matrix D associated with the wedge $W^{B,\ell}$.

In the second case, $w > 1$. Now the children squares have directional equivalent charges as well. The M2M translation iterates over all of the directional indices $\{\ell\}$ of B . The steps for a fixed direction ℓ are as follows:

1. Pick ℓ' , a direction associated with the squares of width $w/2$, such that the wedge $W^{B,\ell}$ is contained in the wedge $W^{C,\ell'}$ where C stands for anyone of B 's children. The existence of ℓ' is ensured by the way we partition F^B (see Figure 5).
2. Use $\bigcup_C \{y_k^{C,o,\ell'}\}$ as source points in B and $\bigcup_C \{f_k^{C,o,\ell'}\}$ as source charges. Here the union is taken over all the children squares of B .
3. Compute $\{u_k^{B,o,\ell}\}$ at $\{x_k^{B,o,\ell}\}$ with kernel evaluation and then obtain $\{f_k^{B,o,\ell}\}$ by multiplying $\{u_k^{B,o,\ell}\}$ with the matrix D associated with the wedge $W^{B,\ell}$.

The *L2L translation* constructs the incoming check potentials of B 's children from the incoming directional check potentials of B . Again there are two cases to consider. In the first case $w = 1$. The children squares have only nondirectional check potentials. The L2L translation iterates over all of the directional indices $\{\ell\}$ of B , and the steps for a fixed direction ℓ are as follows:

1. Compute $\{f_k^{B,i,\ell}\}$ from $\{u_k^{B,i,\ell}\}$ by multiplying it with the appropriate D matrix.
2. For each child C of the square B , add to $\{u_k^{C,i}\}$ the potentials evaluated at $\{x_k^{C,i}\}$ using $\{f_k^{B,i,\ell}\}$ as the source charges at $\{y_k^{B,i,\ell}\}$.

In the second case, $w > 1$. Now the children squares have directional equivalent charges. The L2L translation iterates over all of the directional indices $\{\ell\}$ of B . The steps for a fixed direction ℓ are as follows:

1. Pick ℓ' , a direction associated with the squares of width $w/2$, such that the wedge $W^{B,\ell}$ is contained in the wedge $W^{C,\ell'}$ where C stands for anyone of B 's children.
2. Compute $\{f_k^{B,i,\ell}\}$ from $\{u_k^{B,i,\ell}\}$ by multiplying it with the appropriate D matrix.

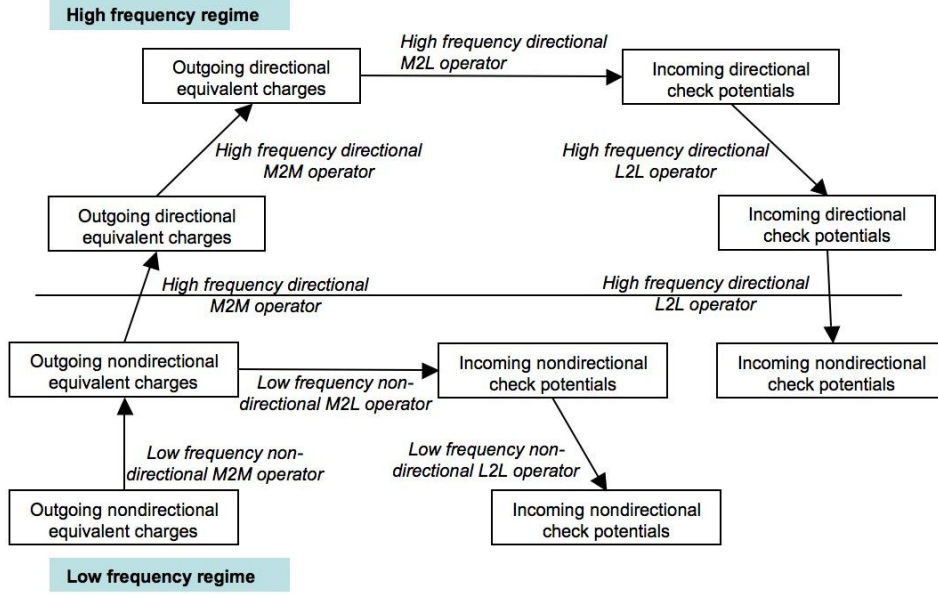


Figure 6: A small part of the quadtree used in the computation. Each rectangular region stands for a square of the quadtree. The diagram shows how the outgoing nondirectional equivalent charges from a leaf square have been transformed into incoming nondirectional check potentials at other leaf squares. Far field interaction involves directional computation in the high frequency regime.

3. For each child C of the square B , add to $\{u_k^{C,i,\ell'}\}$ the potentials evaluated at $\{x_k^{C,i,\ell'}\}$ using $\{f_k^{B,i,\ell}\}$ as the source charges at $\{y_k^{B,i,\ell}\}$.

Finally, the *M2L translation* is applied to pairs of squares A and B on the same level of the quadtree. They need to be on each other's interaction lists. Suppose B falls into the wedge $W^{A,\ell}$ of A while A falls into the wedge $W^{B,\ell'}$ of B . The implementation of the M2L translation contains only one step:

1. Add to $\{u_k^{B,i,\ell'}\}$ the potentials evaluated at $\{x_k^{B,i,\ell'}\}$ using the charges $\{f_k^{A,o,\ell}\}$ at points $\{y_k^{A,o,\ell}\}$.

To summarize the discussion on the transition operators, we would like to emphasize that all of these operators involve only kernel evaluation and matrix-vector multiplication with precomputed matrices. Therefore, they are simple to implement and highly efficient.

3.3 Algorithm

Now we are ready to give the overall structure of our new algorithm. It has exactly the same structure as the 3D algorithm in [15] and we simply reproduce it here:

1. Construct the quadtree. In the high frequency regime, the squares are partitioned uniformly. In the low frequency regime, a leaf square contains at most N_p points.
2. Travel up in the quadtree and visit the squares in the low frequency regime. These squares have width less than 1. For each square B , compute its outgoing nondirec-

tional equivalent charges $\{f_k^{B,o}\}$. This is done using the low frequency nondirectional M2M translation.

3. Travel up in the quadtree and visit the squares in the high frequency regime. For every such square B , use the high frequency directional M2M translation to compute the outgoing directional equivalent charges $\{f_k^{B,o,\ell}\}$ for each outgoing direction ℓ . We skip the squares with width greater than \sqrt{K} since their interaction lists are empty.
4. Travel down in the quadtree and visit the squares in the high frequency regime. For every such square B and for each direction ℓ , perform the following two steps:
 - (a) Transform the outgoing directional equivalent charges $\{f_k^{A,o,\ell}\}$ of all of the squares $\{A\}$ in B 's interaction list and in direction ℓ via the high frequency directional M2L translation. Next, add the result to the incoming directional check potentials $\{u_k^{B,i,\ell}\}$.
 - (b) Perform the high-frequency directional L2L translation to transform $\{u_k^{B,i,\ell}\}$ to the incoming check potentials for B 's children.

Again, we skip the squares with width greater than \sqrt{K} .

5. Travel down in the quadtree. For every square B in the low frequency regime, we perform the following two steps:
 - (a) Transform the outgoing nondirectional equivalent charges $\{f_k^{A,o}\}$ of all of the squares $\{A\}$ in B 's interaction list via the low frequency nondirectional M2L operator. Next, add the result to the incoming nondirectional check potentials $\{u_k^{B,i}\}$.
 - (b) Perform the low frequency directional L2L translation. Depending on whether B is a leaf square or not, add the result to the incoming check potentials of B 's children or to the potentials at the original points inside B .

An illustration of the various components of the algorithm is given in Figure 6. The following theorem summarizes the complexity of the proposed algorithm.

Theorem 3.1. *Let \mathbb{S} be a rectifiable curve in $B(0,1/2)$. Suppose that for a fixed K the points $\{p_i, 1 \leq i \leq N\}$ are samples of $K\mathbb{S}$, where $N = O(K)$ and $K\mathbb{S} = \{K \cdot p, p \in \mathbb{S}\}$ (the surface obtained by magnifying \mathbb{S} by a factor of K). Then, for any prescribed accuracy, the proposed algorithm has a computational complexity $O(K \log K) = O(N \log N)$.*

The proof of this theorem follows closely the steps of Theorem 4.1 of [15]. The main step of the proof is the observation that, for any fixed $w > 1$, there are at most $O(K/w)$ squares of size w and, for each of them, there are at most $O(w)$ squares for which we apply the M2L operator.

4 Numerical Results

In this section, we provide some numerical results to illustrate the properties of our new algorithm. All of the computational results below are obtained on a desktop computer with a 2.8 GHz CPU.

Let us first study the performance of the randomized procedure presented in Section 2. In Table 1, we list the number of terms in the separated representation for two sets X and

	$w = 1$	$w = 2$	$w = 4$	$w = 8$	$w = 16$	$w = 32$	$w = 64$	$w = 128$
$\varepsilon=1e-4$	14	11	11	10	9	9	9	9
$\varepsilon=1e-6$	19	16	14	13	12	12	12	11
$\varepsilon=1e-8$	27	20	16	15	15	15	14	14

Table 1: The separation rank of the directional separated representation for different choices of requested accuracy ε and square size w .

Y for different choices of accuracy ε and square width w . Here r , the radius of Y , is set to be $\sqrt{2}w$ so that the square of width w is contained in Y . We can see from Table 1 that the separation rank is bounded by a constant which is independent of the values of w . This is consistent with our theoretical estimate in Theorem 2.2. In fact, as w grows, it seems that the separation rank decays slightly.

Next, we applied our algorithm to the N -body problems on several objects. In our experiments, the boundary of each object is represented by a piecewise smooth curve. For these tests, the point set $\{p_i\}$ is generated by sampling the curve randomly with about 20 points per wavelength. The densities $\{f_i\}$ are generated from a random distribution with mean 0. We use $\{u_i\}$ to denote the true discrete potentials and $\{u_i^\alpha\}$ to denote the approximations obtained through our algorithm. We estimate the relative error by picking a set S of 200 points from $\{p_i\}$. The true potentials $\{u_i, i \in S\}$ are computed by using direct evaluation. The error is then estimated to be

$$\sqrt{\frac{\sum_{i \in S} |u_i - u_i^\alpha|^2}{\sum_{i \in S} |u_i|^2}}.$$

Before reporting the results, let us summarize the notations we use here: N is the number of points, K is the size of the problem in terms of the wavelength, ε is the prescribed error threshold such that the final error is to be bounded by a constant multiple of ε , T_a is the running time of our algorithm in seconds, T_d is the running time of the direct evaluation in seconds, T_d/T_a is the speedup factor, and ε_a is the resulting error of our algorithm.

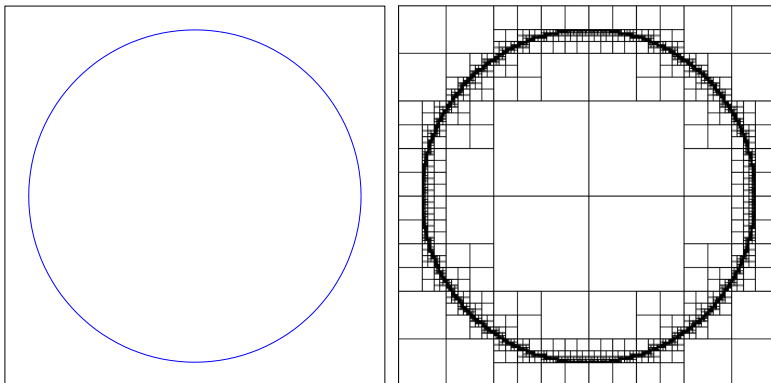
The first example is a circle and the results are summarized in Table 2. The second example is an airfoil and the results are shown in Table 3. The final example is a kite-shaped object and we report the numbers in Table 4. These numbers demonstrate clearly that our algorithm scales exactly like $O(N \log N)$ in terms of the number of points. Furthermore, the error seems to grow only slightly as we increase the number of points.

Compared with the results presented in [7], our algorithm is slower by a factor of 8. The reason is that we heavily use the kernel evaluation formula in our algorithm. The 2D Helmholtz kernel involves the Hankel functions and the current computational procedure for their evaluation is rather slow. On the other hand, all of the high frequency translations in [7] are precomputed and stored in the diagonal form and no special function evaluation is required during the computation.

Finally, we apply our algorithm to the solution of the BIE formulation

$$\frac{1}{2}\phi(x) + \int_{\partial D} \left(\frac{\partial G(x, y)}{\partial n(y)} - \eta G(x, y) \right) \phi(y) dy = -u^{inc}(x)$$

of the 2D scattering problem mentioned in Section 1. Here, we report the numerical results for the smooth objects in Tables 2 and 4. In our experiments, we use a uniform discretization



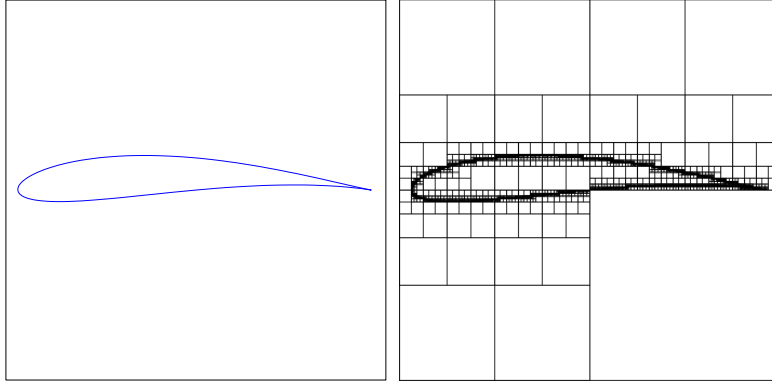
(K, ε)	N	$T_a(\text{sec})$	$T_d(\text{sec})$	T_d/T_a	ε_a
(2048,1e-4)	1.13e+5	3.40e+1	8.05e+3	2.37e+2	1.25e-4
(8192,1e-4)	4.50e+5	1.56e+2	1.28e+5	8.21e+2	1.31e-4
(32768,1e-4)	1.80e+6	7.07e+2	2.06e+6	2.91e+3	1.80e-4
(2048,1e-6)	1.13e+5	5.30e+1	8.00e+3	1.51e+2	7.88e-7
(8192,1e-6)	4.50e+5	2.39e+2	1.28e+5	5.37e+2	9.98e-7
(32768,1e-6)	1.80e+6	1.08e+3	2.06e+6	1.91e+3	1.00e-6
(2048,1e-8)	1.13e+5	8.20e+1	8.05e+3	9.82e+1	8.48e-9
(8192,1e-8)	4.50e+5	3.57e+2	1.29e+5	3.60e+2	1.18e-8
(32768,1e-8)	1.80e+6	1.58e+3	2.07e+6	1.31e+3	1.30e-8

Table 2: Results of a circle with the Helmholtz kernel. N is the number of points, K is the size of the problem in terms of the wavelength, ε is the prescribed error threshold such that the final error is to be bounded by a constant multiple of ε , T_a is the running time of our algorithm in seconds, T_d is the running time of the direct evaluation in seconds, T_d/T_a is the speedup factor, and ε_a is the estimated error of our algorithm.

of about 20 points per wavelength. We pick $\eta = \pi$ and set the incoming field $u^{inc}(x)$ to be $e^{2\pi i x \cdot d}$ with $d = (1, 0)$. We discretize the integral equation with the Nyström method [9, 22] and use the endpoint-corrected trapezoidal rules from [21] to integrate the weakly singular part of the integral. The system is solved iteratively using the GMRES algorithm and the restarted number is set to be 80. Within each iteration of the GMRES solver, the application of the integral operator is accelerated using our multidirectional algorithm with $\varepsilon = 1e-4$. Table 5 summarizes the results for the circle with wavelengths from 1024 to 8192. Here T_i is the averaged time of each iteration, N_i is the number of iterations, and T_t is the total time. Table 6 reports the results of the kite-shaped object in Table 4. In Figure 7, we display the scattering field of the kite-shaped object in a region with caustics.

5 Conclusions

In this paper, we described a directional multiscale algorithm for computing the N -body problem for the high frequency Helmholtz kernel in two dimensions. The approach follows the framework described in [15]. Our algorithm is accurate and works well for problems in all scales. By using the directional low rank representations for regions that follow the directional parabolic separation condition, our algorithm achieves the optimal $O(N \log N)$



(K, ε)	N	$T_a(\text{sec})$	$T_d(\text{sec})$	T_d/T_a	ε_a
(2048,1e-4)	7.82e+4	2.00e+1	3.87e+3	1.94e+2	1.15e-4
(8192,1e-4)	3.13e+5	8.80e+1	6.17e+4	7.02e+2	1.21e-4
(32768,1e-4)	1.25e+6	3.90e+2	9.90e+5	2.54e+3	1.07e-4
(2048,1e-6)	7.82e+4	3.20e+1	3.87e+3	1.21e+2	1.04e-6
(8192,1e-6)	3.13e+5	1.38e+2	6.20e+4	4.50e+2	9.65e-7
(32768,1e-6)	1.25e+6	6.05e+2	1.01e+6	1.67e+3	1.20e-6
(2048,1e-8)	7.82e+4	4.70e+1	3.87e+3	8.24e+1	8.58e-9
(8192,1e-8)	3.13e+5	2.03e+2	6.22e+4	3.06e+2	1.69e-8
(32768,1e-8)	1.25e+6	8.78e+2	9.95e+5	1.13e+3	1.33e-8

Table 3: Results of an airfoil with the Helmholtz kernel.

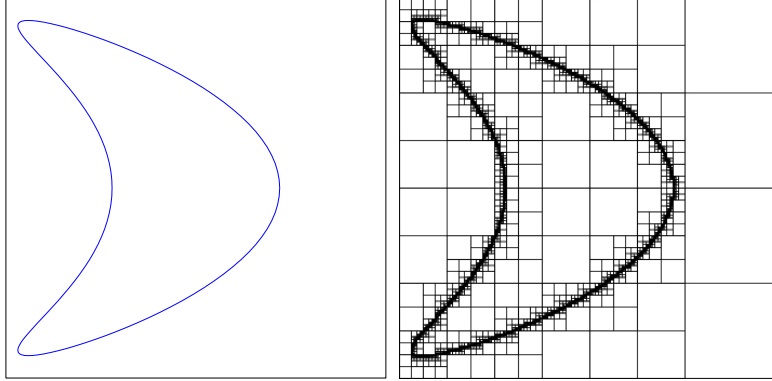
complexity. A new and more efficient randomized technique compared to the one in [15] has also been introduced for the construction of the low rank separated representations. The numerical results have shown that our algorithm is capable of addressing very large scale problems in high frequency scattering.

For future work, we would like to have a rigorous proof for the randomized procedure proposed in Section 2. Another interesting direction for future research is to apply this kind of directional multiscale idea to other problems with oscillatory behavior, in both two and three dimensions. One typical example is the computation of the far field pattern of a scattering field [9, 29].

Acknowledgments. The authors would like to thank P.G. Martinsson for helpful discussions. B.E. is partially supported by an NSF grant DMS 0714612 and a startup grant from the University of Texas at Austin. L.Y. is partially supported by an Alfred P. Sloan Research Fellowship and a startup grant from the University of Texas at Austin.

References

- [1] M. Abramowitz and I. A. Stegun, editors. *Handbook of mathematical functions with formulas, graphs, and mathematical tables*. Dover Publications Inc., New York, 1992. Reprint of the 1972 edition.
- [2] A. Averbuch, E. Braverman, R. Coifman, M. Israeli, and A. Sidi. Efficient computation of oscillatory integrals via adaptive multiscale local Fourier bases. *Appl. Comput. Harmon. Anal.*, 9(1):19–53, 2000.



(K, ε)	N	$T_a(\text{sec})$	$T_d(\text{sec})$	T_d/T_a	ε_a
(2048,1e-4)	1.13e+5	4.00e+1	8.11e+3	2.03e+2	1.08e-4
(8192,1e-4)	4.53e+5	1.77e+2	1.30e+5	7.36e+2	1.33e-4
(32768,1e-4)	1.81e+6	8.04e+2	2.09e+6	2.60e+3	1.41e-4
(2048,1e-6)	1.13e+5	6.10e+1	8.11e+3	1.33e+2	9.35e-7
(8192,1e-6)	4.53e+5	2.72e+2	1.30e+5	4.78e+2	9.15e-7
(32768,1e-6)	1.81e+6	1.24e+3	2.10e+6	1.70e+3	8.80e-7
(2048,1e-8)	1.13e+5	9.20e+1	8.16e+3	8.87e+1	1.45e-8
(8192,1e-8)	4.53e+5	4.05e+2	1.30e+5	3.22e+2	1.31e-8
(32768,1e-8)	1.81e+6	1.80e+3	2.11e+6	1.17e+3	1.52e-8

Table 4: Results of a kite-shaped model with the Helmholtz kernel.

- [3] M. Bebendorf and S. Rjasanow. Adaptive low-rank approximation of collocation matrices. *Computing*, 70(1):1–24, 2003.
- [4] B. Bradie, R. Coifman, and A. Grossmann. Fast numerical computations of oscillatory integrals related to acoustic scattering. I. *Appl. Comput. Harmon. Anal.*, 1(1):94–99, 1993.
- [5] I. N. Bronshtein and K. A. Semendyayev. *Handbook of mathematics*. Springer-Verlag, Berlin, english edition, 1997. Translated from the German, Translation edited by K. A. Hirsch.
- [6] F. X. Canning. Sparse approximation for solving integral equations with oscillatory kernels. *SIAM J. Sci. Statist. Comput.*, 13(1):71–87, 1992.
- [7] H. Cheng, W. Crutchfield, Z. Gimbutas, L. Greengard, J. Huang, V. Rokhlin, N. Yarvin, and J. Zhao. Remarks on the implementation of the wideband FMM for the Helmholtz equation in two dimensions. In *Inverse problems, multi-scale analysis and effective medium theory*, volume 408 of *Contemp. Math.*, pages 99–110. Amer. Math. Soc., Providence, RI, 2006.
- [8] H. Cheng, Z. Gimbutas, P. G. Martinsson, and V. Rokhlin. On the compression of low rank matrices. *SIAM J. Sci. Comput.*, 26(4):1389–1404, 2005.
- [9] D. L. Colton and R. Kress. *Integral equation methods in scattering theory*. Pure and Applied Mathematics (New York). John Wiley & Sons Inc., New York, 1983.

K	N	$T_i(\text{sec})$	N_i	$T_t(\text{sec})$
1024	65536	22	72	1.60e+3
2048	131072	45	93	4.32e+3
4096	262144	99	118	1.20e+4
8192	524288	202	150	3.12e+4

Table 5: Timings of computing the scattering field of the circle. K is the size of the problem in terms of the wavelength, N is the number of quadrature points, T_i is the averaged time of each iteration, N_i is the number of iterations, and T_t is the total time.

K	N	$T_i(\text{sec})$	N_i	$T_t(\text{sec})$
1024	65536	22	227	5.11e+3
2048	131072	46	314	1.49e+4
4096	262144	99	435	4.42e+4
8192	524288	204	604	1.25e+5

Table 6: Timings of computing the scattering field of the kite-shaped object.

- [10] S. Dasgupta and A. Gupta. An elementary proof of a theorem of johnson and lindenstrauss. *Random Struct. Algorithms*, 22(1):60–65, 2003.
- [11] H. Deng and H. Ling. Fast solution of electromagnetic integral equations using adaptive wavelet packet transform. *Antennas and Propagation, IEEE Transactions on*, 47(4):674–682, Apr 1999.
- [12] H. Deng and H. Ling. On a class of predefined wavelet packet bases for efficient representation of electromagnetic integral equations. *Antennas and Propagation, IEEE Transactions on*, 47(12):1772–1779, Dec 1999.
- [13] P. Drineas, R. Kannan, and M. W. Mahoney. Fast Monte Carlo algorithms for matrices. II. Computing a low-rank approximation to a matrix. *SIAM J. Comput.*, 36(1):158–183, 2006.
- [14] P. Drineas, R. Kannan, and M. W. Mahoney. Fast Monte Carlo algorithms for matrices. III. Computing a compressed approximate matrix decomposition. *SIAM J. Comput.*, 36(1):184–206, 2006.
- [15] B. Engquist and L. Ying. Fast directional multilevel algorithms for oscillatory kernels. *SIAM Journal on Scientific Computing*, 29(4):1710–1737, 2007.
- [16] W. Golik. Wavelet packets for fast solution of electromagnetic integral equations. *Antennas and Propagation, IEEE Transactions on*, 46(5):618–624, May 1998.
- [17] S. A. Goreinov, E. E. Tyrtyshnikov, and N. L. Zamarashkin. A theory of pseudoskeleton approximations. *Linear Algebra Appl.*, 261:1–21, 1997.
- [18] S. A. Goreinov, N. L. Zamarashkin, and E. E. Tyrtyshnikov. Pseudoskeleton approximations by submatrices of greatest size. *Mat. Zametki*, 62(4):619–623, 1997.
- [19] L. Greengard and V. Rokhlin. A fast algorithm for particle simulations. *J. Comput. Phys.*, 73(2):325–348, 1987.

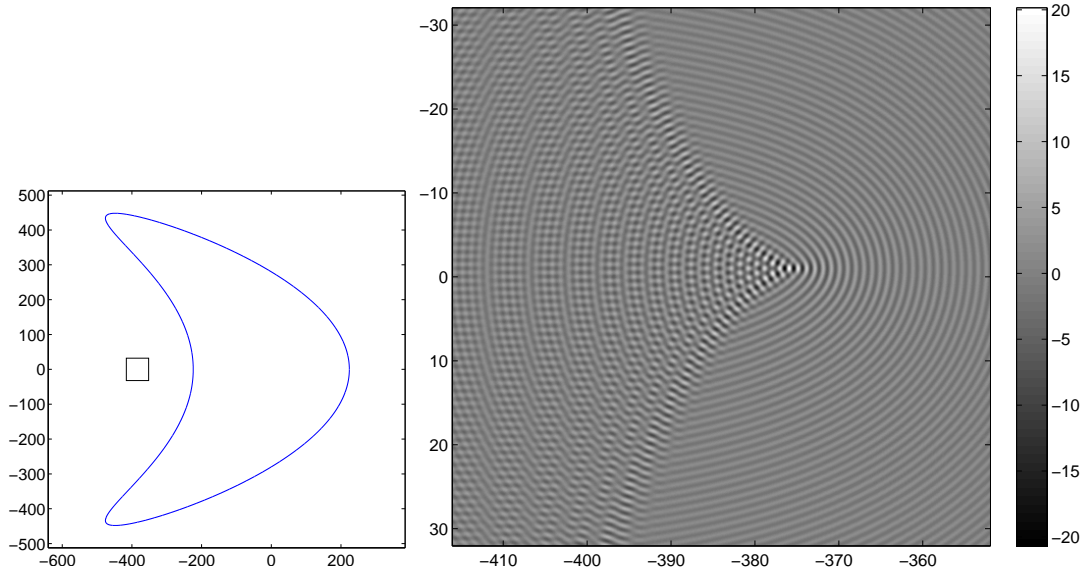


Figure 7: Scattering field of the kite-shaped object with $K = 1024$. Top: a square region that contains the caustics. Bottom: the real part of the scattering field inside the square. The field is sampled at 8 points per wavelength.

- [20] D. Huybrechs and S. Vandewalle. A two-dimensional wavelet-packet transform for matrix compression of integral equations with highly oscillatory kernel. *J. Comput. Appl. Math.*, 197(1):218–232, 2006.
- [21] S. Kapur and V. Rokhlin. High-order corrected trapezoidal quadrature rules for singular functions. *SIAM J. Numer. Anal.*, 34(4):1331–1356, 1997.
- [22] R. Kress. *Linear integral equations*, volume 82 of *Applied Mathematical Sciences*. Springer-Verlag, New York, second edition, 1999.
- [23] A. Magen. Dimensionality reductions that preserve volumes and distance to affine spaces, and their algorithmic applications. In J. D. P. Rolim and S. P. Vadhan, editors, *RANDOM*, volume 2483 of *Lecture Notes in Computer Science*, pages 239–253. Springer, 2002.
- [24] P.-G. Martinsson, V. Rokhlin, and M. Tygert. A randomized algorithm for the approximation of matrices. Technical report, Yale University, 2006.
- [25] E. Michielssen and A. Boag. A multilevel matrix decomposition algorithm for analyzing scattering from large structures. *IEEE Transactions on Antennas and Propagation*, 44(8):1086–1093, 1996.
- [26] M. O’Neil and V. Rokhlin. A new class of analysis-based fast transforms. Technical report, Yale University. YALE/DCS/TR1384, 2007.
- [27] V. Rokhlin. Rapid solution of integral equations of scattering theory in two dimensions. *J. Comput. Phys.*, 86(2):414–439, 1990.

- [28] Y. Saad and M. H. Schultz. GMRES: a generalized minimal residual algorithm for solving nonsymmetric linear systems. *SIAM J. Sci. Statist. Comput.*, 7(3):856–869, 1986.
- [29] L. Ying. Sparse Fourier transform via butterfly algorithm. Technical report, University of Texas at Austin, 2007.
- [30] L. Ying, G. Biros, and D. Zorin. A kernel-independent adaptive fast multipole algorithm in two and three dimensions. *J. Comput. Phys.*, 196(2):591–626, 2004.